Design of robust concentric circular differential microphone arrays

Gongping Huang, Jacob Benesty, and Jingdong Chen

Citation: The Journal of the Acoustical Society of America **141**, 3236 (2017); doi: 10.1121/1.4983122
View online: https://doi.org/10.1121/1.4983122
View Table of Contents: https://asa.scitation.org/toc/jas/141/5
Published by the Acoustical Society of America

Design of robust concentric circular differential microphone arrays

Gongping Huang
Center of Intelligent Acoustics and Immersive Communications and School of Marine Science and Technology, Northwestern Polytechnical University, 127 Youyi West Road, Xi'an 710072, China

Jacob Benesty
INRS-EMT, University of Quebec, 800 de la Gauchetiere Ouest, Montreal, QC H5A 1K6, Canada

Jingdong Chen[a)]
Center of Intelligent Acoustics and Immersive Communications, Northwestern Polytechnical University, 127 Youyi West Road, Xi'an 710072, China

(Received 19 October 2016; revised 10 April 2017; accepted 25 April 2017; published online 16 May 2017)

Circular differential microphone arrays (CDMAs) have been extensively studied in speech and audio applications for their steering flexibility, potential to achieve frequency-invariant directivity patterns, and high directivity factors (DFs). However, CDMAs suffer from both white noise amplification and deep nulls in the DF and in the white noise gain (WNG) due to spatial aliasing, which considerably restricts their use in practical systems. The minimum-norm filter can improve the WNG by using more microphones than required for a given differential array order; but this filter increases the array aperture (radius), which exacerbates the spatial aliasing problem and worsens the nulls problem in the DF. Through theoretical analysis, this research finds that the nulls of the CDMAs are caused by the zeros in the denominators of the filters' coefficients, i.e., the zeros of the Bessel function. To deal with both the white noise amplification and deep nulls problems, this paper develops an approach that combines different rings of microphones together with appropriate radii. The resulting robust concentric circular differential microphone arrays (CCDMAs) can mitigate both problems. Simulation results justify the superiority of the robust CCDMA approach over the traditional CDMAs and robust CDMAs.
[http://dx.doi.org/10.1121/1.4983122]

[JFL] Pages: 3236–3249

I. INTRODUCTION

Microphone arrays, combined with proper signal processing algorithms, can be used to solve many important acoustic problems such as extracting a signal of interest, reducing the negative effects of noise, reverberation, and interference on the speech signal of interest, and separating different sound sources (Brandstein and Ward, 2001; Benesty *et al.*, 2008; Gannot *et al.*, 1999; Huang *et al.*, 2016; Shahbazpanahi *et al.*, 2003; Markovich *et al.*, 2009; Benesty *et al.*, 2012; Elko, 1996; Wang *et al.*, 2014). The design of microphone arrays and the associated beamforming algorithms have attracted a significant amount of research attention, and many beamformers such as the delay-and-sum (DS), filter-and-sum, superdirective, and differential have been developed over the past few decades (Capon, 1969; Frost, 1972; Van Veen and Buckley, 1988; Cox *et al.*, 1987; Crocco and Trucco, 2011; Berkun *et al.*, 2015; Li *et al.*, 2016; Doclo and Moonen, 2007; Quijano and Zurk, 2015).

Although it has been successfully used in narrowband applications, beamforming with microphone arrays is less successful because speech and audio signals are broadband in nature with a frequency range from 20 Hz to approximately 20 kHz (Brandstein and Ward, 2001; Benesty *et al.*, 2008; Benesty and Chen, 2012). With such broadband signals, the conventional beamformers' beamwidth is inversely proportional to the frequency (for instance, the conventional DS beamformer's beam is wider at low than at high frequencies) and, as a result, those beamformers are not effective in dealing with noise and interference at low frequencies. Moreover, noise is not uniformly attenuated over its entire spectrum, resulting in some disturbing artifacts in the array output (Benesty and Chen, 2012). Therefore, how to design a broadband beamformer that can work consistently in such a large frequency range is a very difficult and challenging issue.

Several techniques have been developed to achieve broadband beamforming, such as nested arrays, mode based beamforming (Rafaely, 2005; Poletti, 2000; Park and Rafaely, 2005; Rafaely *et al.*, 2007; Teutsch and Kellermann, 2006; Teutsch, 2007; Tiana-Roig *et al.*, 2010; Sun *et al.*, 2012; Yan, 2015; Koyama *et al.*, 2016), and differential beamforming (Balmages and Rafaely, 2007; Ihle, 2003; Benesty and Chen, 2012; Zhao *et al.*, 2014). Among them, differential beamforming has attracted much interest since it has the potential to achieve frequency-invariant beampatterns and high directivity factors (DFs) (Teutsch and Elko, 2001; Sena *et al.*, 2012; Elko, 2004; Olson, 1946; Abhayapala and Gupta, 2010; Zhao *et al.*, 2014). Conventional differential microphone arrays (DMAs) are designed in a multistage manner, which

[a)]Electronic mail: jingdongchen@ieee.org.

lack flexibility in forming different beampatterns and suffer from significant white noise amplification. Recently, a new approach was developed for the design and implementation of linear differential microphone arrays (LDMAs) with some null information from the desired beampatterns (Benesty and Chen, 2012). This method is much more flexible to design different directivity patterns and offers significant advantages over the conventional DMAs. More importantly, this approach can deal with the white noise amplification problem by increasing the number of microphones as compared to the DMA order (Benesty and Chen, 2012). This idea was further extended to the design of circular differential microphone arrays (CDMAs) in Benesty *et al.* (2014). A great advantage of CDMAs as compared to LDMAs is that their beam can be electronically steered and is expected to have a similar directional gain in different directions (Benesty *et al.*, 2014), which can be useful when the signal of interest may come from other directions than the endfires (Chan and Chen, 2007; Tiana-Roig *et al.*, 2011). Another important advantage of circular arrays is that the processing can be greatly simplified due to the inherent symmetry (Benesty *et al.*, 2014).

Similarly, CDMAs suffer from white noise amplification and the minimum-norm filter can be used to improve the white noise gain (WNG). Besides white noise amplification, CDMAs also suffer from deep nulls in the DF and in the WNG due to spatial aliasing, implying serious degradation in signal-to-noise ratio (SNR) gain at certain frequencies. While it can improve the WNG, the minimum-norm filter may worsen the SNR gain degradation caused by the nulls. The major underlying reason is that the minimum-norm filter improves the WNG by using more microphones than required for the order of the differential array, which generally leads to a larger array aperture. Consequently, more nulls appear in the frequency band of interest and the nulls' positions move to lower frequencies.

Through both theoretical analysis and experimental studies, we find in our study that the nulls of CDMAs are caused by the zeros in the denominators of the filters' coefficients, i.e., the zeros of the Bessel function. To design an *N*th-order CDMA, any zero of the Bessel functions of any order will cause a deep null in the SNR gains. To circumvent this issue, this paper proposes a robust concentric circular differential microphone arrays (CCDMA) approach, which can improve the WNG without introducing any nulls. The reason is that a uniform concentric circular array (UCCA) is a combination of several rings together with appropriate radii; as a result, the corresponding filter's coefficients are also a combination of different Bessel functions and, since the zeros of this function are occurring at different frequencies, the combined function does not have any nulls. Consequently, the robust CCDMA can achieve consistent performance over the frequency band of interest and performs better than CDMAs.

The organization of this paper is as follows. In Sec. II, we explain the signal model and the problem of beamforming. Section III presents some important performance measures. Section IV shows how the beampattern of a beamformer with a UCCA is related to the definition of a theoretical *N*th-order DMA directivity pattern. Section V presents algorithms of designing the robust CCDMA. In Sec. VI, we present some simulations to validate the theoretical analysis. Finally, some conclusions are drawn in Sec. VII.

II. SIGNAL MODEL AND PROBLEM FORMULATION

We consider a UCCA with P rings, placed on the $x-y$ plane, where the pth ($p = 1, 2, \ldots, P$) ring, with a radius of r_p, consists of M_p omnidirectional microphones. We assume that the center of the UCCA coincides with the origin of the two-dimensional Cartesian coordinate system, azimuthal angles are measured anti-clockwise from the x axis, and sensor 1 of the array is placed on the x axis (as shown in Fig. 1). Then, the coordinates of the mth microphone at the pth ring are written as

$$\mathbf{r}_{p,m} = (r_p \cos\psi_{p,m}, r_p \sin\psi_{p,m}), \quad (1)$$

where $p = 1, 2, \ldots, P$, $m = 1, 2, \ldots, M_p$, and

$$\psi_{p,m} = \frac{2\pi(m-1)}{M_p} \quad (2)$$

is the angular position of the mth array element on the pth ring. We assume that a source signal (plane wave) located in the farfield impinges on the UCCA from the direction (azimuth angle) θ_s, at the speed of sound in the air, e.g., $c = 340$ m/s. Suppose that we want to steer the beam to the direction θ, the steering vector of length $\underline{M}$, where $\underline{M} = \sum_{p=1}^{P} M_p$ is the total number of microphones, is then defined as (Monzingo and Miller, 1980)

$$\underline{\mathbf{d}}(\omega,\theta) \triangleq \left[\, \mathbf{d}_1^T(\omega,\theta) \quad \mathbf{d}_2^T(\omega,\theta) \cdots \mathbf{d}_P^T(\omega,\theta) \,\right]^T, \quad (3)$$

where

$$\mathbf{d}_p(\omega,\theta) \triangleq \left[e^{\jmath\varpi_p \cos(\theta-\psi_{p,1})} \; e^{\jmath\varpi_p \cos(\theta-\psi_{p,2})} \cdots \; e^{\jmath\varpi_p \cos(\theta-\psi_{p,M_p})} \right]^T \quad (4)$$

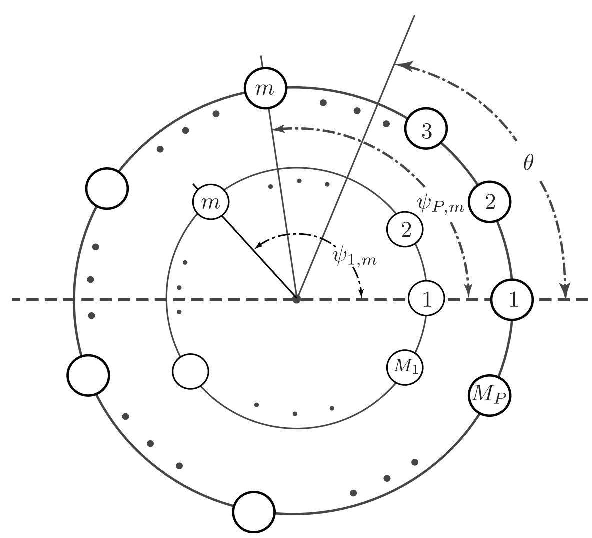

FIG. 1. Illustration of a UCCA with P rings, where the pth ($p = 1, 2, \ldots, P$) ring, with a radius of r_p, consists of M_p omnidirectional microphones, with $\psi_{p,m}$ being the angular position of the mth array element on the pth ring and θ being the source incidence angle.

is the pth ring's steering vector, the superscript ^{T} is the transpose operator, $\jmath$ is the imaginary unit with $\jmath^2 = -1$, and

$$\varpi_p \triangleq \frac{\omega r_p}{c}, \tag{5}$$

with $\omega = 2\pi f$ being the angular frequency and $f > 0$ being the temporal frequency.

To simplify the exposition, we assume that the desired signal comes from the direction $\theta_s = \theta = 0$. Then, the received frequency-domain signal by the mth microphone at the pth ring is

$$Y_{p,m}(\omega) = e^{\jmath\varpi_p \cos(\psi_{p,m})} X(\omega) + V_{p,m}(\omega), \tag{6}$$

where $X(\omega)$ is the desired signal and $V_{p,m}(\omega)$ is the additive noise. In a vector form for the pth ring, we have

$$\begin{aligned} \mathbf{y}_p(\omega) &\triangleq \begin{bmatrix} Y_{p,1}(\omega) & Y_{p,2}(\omega) & \cdots & Y_{p,M_p}(\omega) \end{bmatrix}^T \\ &= \mathbf{x}_p(\omega) + \mathbf{v}_p(\omega) \\ &= \mathbf{d}_p(\omega)X(\omega) + \mathbf{v}_p(\omega), \end{aligned} \tag{7}$$

where $\mathbf{x}_p(\omega) = \mathbf{d}_p(\omega)X(\omega)$, $\mathbf{d}_p(\omega) = \mathbf{d}_p(\omega, 0)$, and $\mathbf{v}_p(\omega)$ is defined similarly to $\mathbf{y}_p(\omega)$. It is more convenient to concatenate the P vectors $\mathbf{y}_p(\omega)$, $p = 1, 2, \ldots, P$, together as

$$\begin{aligned} \underline{\mathbf{y}}(\omega) &\triangleq \begin{bmatrix} \mathbf{y}_1^T(\omega) & \mathbf{y}_2^T(\omega) & \cdots & \mathbf{y}_P^T(\omega) \end{bmatrix}^T \\ &= \underline{\mathbf{x}}(\omega) + \underline{\mathbf{v}}(\omega) \\ &= \underline{\mathbf{d}}(\omega)X(\omega) + \underline{\mathbf{v}}(\omega), \end{aligned} \tag{8}$$

where $\underline{\mathbf{x}}(\omega) = \underline{\mathbf{d}}(\omega)X(\omega)$, $\underline{\mathbf{d}}(\omega) = \underline{\mathbf{d}}(\omega, 0)$, and $\underline{\mathbf{v}}(\omega)$ is defined in a similar way to $\underline{\mathbf{y}}(\omega)$.

Beamforming consists of applying a complex weight, $H^*_{p,m}(\omega)$, where the superscript * denotes complex conjugation, to the microphone's output, $Y_{p,m}(\omega)$, and then summing all the weighted outputs together to get an estimate of the desired signal (Benesty *et al.*, 2008), i.e.,

$$\begin{aligned} Z(\omega) &= \sum_{p=1}^{P}\sum_{m=1}^{M_p} H^*_{p,m}(\omega)Y_{p,m}(\omega) \\ &= \underline{\mathbf{h}}^H(\omega)\underline{\mathbf{y}}(\omega) \\ &= \underline{\mathbf{h}}^H(\omega)\underline{\mathbf{d}}(\omega)X(\omega) + \underline{\mathbf{h}}^H(\omega)\underline{\mathbf{v}}(\omega), \end{aligned} \tag{9}$$

where

$$\underline{\mathbf{h}}(\omega) \triangleq \begin{bmatrix} \mathbf{h}_1^T(\omega) & \mathbf{h}_2^T(\omega) & \cdots & \mathbf{h}_P^T(\omega) \end{bmatrix}^T \tag{10}$$

is the global spatial filter of length $\underline{M}$, the superscript ^{H} is the conjugate-transpose operator, and

$$\mathbf{h}_p(\omega) \triangleq \begin{bmatrix} H_1(\omega) & H_2(\omega) & \cdots & H_{M_p}(\omega) \end{bmatrix}^T \tag{11}$$

is the spatial filter of length M_p for the pth ring.

In our context, the array gain in the look direction is expected to be 1, i.e., we should have

$$\underline{\mathbf{h}}^H(\omega)\underline{\mathbf{d}}(\omega) = 1. \tag{12}$$

III. PERFORMANCE MEASURES

The performance of a beamformer is generally evaluated through the signal-to-noise ratio (SNR) gain. Without loss of generality, we consider the first microphone on the first ring as the reference. The input SNR is then defined as

$$i\mathrm{SNR}(\omega) \triangleq \frac{\phi_X(\omega)}{\phi_V(\omega)} \tag{13}$$

where $\phi_X(\omega) \triangleq E[|X(\omega)|^2]$ and $\phi_V(\omega) \triangleq E[|V_{1,1}(\omega)|^2]$ are the variances of $X(\omega)$ and $V_{1,1}(\omega)$, respectively, with $E[\cdot]$ denoting mathematical expectation. The output SNR, according to (9), is given by

$$\begin{aligned} \mathrm{oSNR}[\underline{\mathbf{h}}(\omega)] &= \frac{\phi_X(\omega)|\underline{\mathbf{h}}^H(\omega)\underline{\mathbf{d}}(\omega)|^2}{\underline{\mathbf{h}}^H(\omega)\mathbf{\Phi}_{\underline{\mathbf{v}}}(\omega)\underline{\mathbf{h}}(\omega)} \\ &= \frac{\phi_X(\omega)}{\phi_V(\omega)} \times \frac{|\underline{\mathbf{h}}^H(\omega)\underline{\mathbf{d}}(\omega)|^2}{\underline{\mathbf{h}}^H(\omega)\mathbf{\Gamma}_{\underline{\mathbf{v}}}(\omega)\underline{\mathbf{h}}(\omega)}, \end{aligned} \tag{14}$$

where $\mathbf{\Phi}_{\underline{\mathbf{v}}}(\omega) \triangleq E[\underline{\mathbf{v}}(\omega)\underline{\mathbf{v}}^H(\omega)]$ and $\mathbf{\Gamma}_{\underline{\mathbf{v}}}(\omega) \triangleq \mathbf{\Phi}_{\underline{\mathbf{v}}}(\omega)/\phi_V(\omega)$ are the correlation and pseudo-coherence matrices (Benesty and Gänsler, 2002) of $\underline{\mathbf{v}}(\omega)$, respectively. It follows from (13) and (14) immediately that the SNR gain is

$$\begin{aligned} \mathcal{G}[\underline{\mathbf{h}}(\omega)] &\triangleq \frac{\mathrm{oSNR}[\underline{\mathbf{h}}(\omega)]}{\mathrm{iSNR}(\omega)} \\ &= \frac{|\underline{\mathbf{h}}^H(\omega)\underline{\mathbf{d}}(\omega)|^2}{\underline{\mathbf{h}}^H(\omega)\mathbf{\Gamma}_{\underline{\mathbf{v}}}(\omega)\underline{\mathbf{h}}(\omega)}. \end{aligned} \tag{15}$$

In our discussion, we consider two important scenarios.

- The temporally and spatially white noise with the same variance at all microphones.[1] In this case, $\mathbf{\Gamma}_{\underline{\mathbf{v}}}(\omega) = \mathbf{I}_{\underline{M}}$, where $\mathbf{I}_{\underline{M}}$ is the $\underline{M} \times \underline{M}$ identity matrix. Therefore, the SNR gain is

$$\mathcal{W}[\underline{\mathbf{h}}(\omega)] = \frac{|\underline{\mathbf{h}}^H(\omega)\underline{\mathbf{d}}(\omega)|^2}{\underline{\mathbf{h}}^H(\omega)\underline{\mathbf{h}}(\omega)}, \tag{16}$$

  which is called the white noise gain (WNG) (Brandstein and Ward, 2001).
- The diffuse noise (this situation corresponds to the spherically isotropic noise field). In this case, the coherence between the noise at any two points is a function of the distance between the sensors, where the (i, j)th element of the noise pseudo-coherence matrix is

$$\left[\mathbf{\Gamma}_{\underline{\mathbf{v}}}(\omega)\right]_{ij} = [\mathbf{\Gamma}_{\mathrm{dn}}(\omega)]_{ij} = \mathrm{sinc}\left(\frac{\omega\delta_{ij}}{c}\right), \tag{17}$$

  with

$$\delta_{ij} \triangleq ||\mathbf{r}_i - \mathbf{r}_j||_2 \tag{18}$$

  being the distance between microphones i and j, $||\cdot||_2$ being the Euclidean norm, and $\mathbf{r}_i, \mathbf{r}_j \in \{\mathbf{r}_{1,1}, \mathbf{r}_{1,2}, \ldots, \mathbf{r}_{p,M_p}, \ldots, \mathbf{r}_{P,M_P}\}$ are coordinates of the microphones as defined in (1). Now, the SNR gain is

$$\mathcal{D}[\underline{\mathbf{h}}(\omega)] = \frac{|\underline{\mathbf{h}}^H(\omega)\underline{\mathbf{d}}(\omega)|^2}{\underline{\mathbf{h}}^H(\omega)\mathbf{\Gamma}_{\mathrm{dn}}(\omega)\underline{\mathbf{h}}(\omega)}, \tag{19}$$

which is called the directivity factor (DF) (Elko and Meyer, 2008).

The beampattern or directivity pattern describes the sensitivity of the beamformer to a plane wave impinging on the array from the direction θ. Mathematically, the beampattern with a UCCA is defined as

$$\begin{aligned}\mathcal{B}[\underline{\mathbf{h}}(\omega),\theta] &\triangleq \underline{\mathbf{h}}^H(\omega)\underline{\mathbf{d}}(\omega,\theta)\\ &= \sum_{p=1}^{P}\mathbf{h}_p^H(\omega)\mathbf{d}_p(\omega,\theta)\\ &= \sum_{p=1}^{P}\sum_{m=1}^{M_p}H_{p,m}^*(\omega)e^{\jmath\varpi_p\cos(\theta-\psi_{p,m})}.\end{aligned} \tag{20}$$

IV. RELATIONSHIP BETWEEN THE BEAMPATTERN OF THE BEAMFORMER AND THE THEORETICAL DMA DIRECTIVITY PATTERN

In this section, we show how the beampattern of the beamformer with a UCCA is related to the theoretical Nth-order DMA directivity pattern.

A. Theoretical *N*th-order DMA directivity pattern

The frequency-independent Nth-order DMA directivity pattern is (Benesty and Chen, 2012; Benesty *et al.*, 2014)

$$\mathcal{B}_N(\theta) = \sum_{n=0}^{N} b_{N,n}\cos(n\theta), \tag{21}$$

where $b_{N,n}$, $n = 0, 1, \ldots, N$ are real coefficients and the different values of these coefficients determine the different directivity patterns of the Nth-order DMA. In the direction of the desired signal, i.e., for $\theta = 0$, the beampattern should be equal to 1, i.e., $\mathcal{B}_N(0) = 1$. Therefore, we have

$$\sum_{n=0}^{N} b_{N,n} = 1. \tag{22}$$

From (21), it is seen that a differential beamformer must have a symmetric beampattern, i.e., $\mathcal{B}_N(-\theta) = \mathcal{B}_N(\theta)$. In order to be able to design a CCDMA beamformer, its beampattern must be an even function (Benesty *et al.*, 2014), i.e., we must have

$$\mathcal{B}[\underline{\mathbf{h}}(\omega),\theta] = \mathcal{B}[\underline{\mathbf{h}}(\omega),-\theta]. \tag{23}$$

We recall that we use a UCCA with P rings. This configuration is effective and practical since it has the flexibility of adjusting the number of rings and microphones. From (2), we have the following relations (Benesty *et al.*, 2014):

$$\cos(\theta+\psi_{p,m+1}) = \cos(\theta-\psi_{p,M_p-m+1}), \tag{24}$$

where $p = 1, 2, \ldots, P$, $m = 1, 2, \ldots, M_p$. Substituting (24) into the beampattern of the beamformer given in (20), we find that (23) is true if and only if the following relations hold (Benesty *et al.*, 2014):

$$H_{p,m+1}(\omega) = H_{p,M_p-m+1}(\omega), \tag{25}$$

where $p = 1, 2, \ldots, P$, $m = 1, 2, \ldots, \mathcal{M}_p$ ($\mathcal{M}_p = \lfloor M_p/2\rfloor + 1$, where $\lfloor\cdot\rfloor$ stands for the integer part). We observe that in the filter $\mathbf{h}_p(\omega)$ of length M_p, only its first $\mathcal{M}_p$ coefficients need to be optimized, and the rest will be determined according to the symmetry property in (25).

B. Relationship between the beampattern of the beamformer with a UCCA and the theoretical DMA directivity pattern

Substituting (24) into (20) and using the symmetry property in (25), we can rewrite the beampattern as

$$\begin{aligned}\mathcal{B}[\underline{\mathbf{h}}(\omega),\theta] &= \sum_{p=1}^{P}\sum_{m=1}^{M_p}H_{p,m}^*(\omega)e^{\jmath\varpi_p\cos(\theta-\psi_{p,m})}\\ &= \sum_{p=1}^{P}\sum_{m=1}^{\mathcal{M}_p}H'^*_{p,m}(\omega)\\ &\quad\times\left[e^{\jmath\varpi_p\cos(\theta-\psi_{p,m})}+e^{\jmath\varpi_p\cos(\theta+\psi_{p,m})}\right],\end{aligned} \tag{26}$$

where

$$\begin{aligned}H'_{p,m}(\omega) &= \begin{cases}\frac{1}{2}H_{p,m}, & m=1\\ H_{p,m}, & m = 2,\ldots,\mathcal{M}_p-1,\end{cases}\\ H'_{p,\mathcal{M}_p}(\omega) &= \begin{cases}H_{p,\mathcal{M}_p} & (\text{if } M_p \text{ odd})\\ \frac{1}{2}H_{p,\mathcal{M}_p} & (\text{if } M_p \text{ even}).\end{cases}\end{aligned} \tag{27}$$

To establish the relationship between the beampattern of the beamformer with a UCCA and the theoretical Nth-order DMA directivity pattern, we use the Jacobi-Anger expansion (Benesty *et al.*, 2014; Abramowitz and Stegun, 1972; Zhao *et al.*, 2016):

$$e^{\jmath\varpi_p\cos(\theta\pm\psi_{p,m})} = J_0(\varpi_p) + \sum_{n=1}^{\infty}2\jmath^n J_n(\varpi_p)\cos\left[n(\theta\pm\psi_{p,m})\right], \tag{28}$$

where $J_n(\varpi_p)$ is the nth-order Bessel function of the first kind. Assuming that ϖ_p (or r_p) is small, it can be approximated up to its Nth order, i.e.,

$$\begin{aligned}e^{\jmath\varpi_p\cos(\theta\pm\psi_{p,m})} &\approx J_0(\varpi_p) + \sum_{n=1}^{N}2\jmath^n J_n(\varpi_p)\cos\left[n(\theta\pm\psi_{p,m})\right]\\ &= \sum_{n=0}^{N}J'_n(\varpi_p)\cos\left[n(\theta\pm\psi_{p,m})\right],\end{aligned} \tag{29}$$

where

$$J'_n(\varpi_p) = \begin{cases} J_n(\varpi_p), & n = 0 \\ 2\jmath^n J_n(\varpi_p), & n = 1, 2, \ldots, N. \end{cases} \quad (30)$$

From above, it is not difficult to verify that

$$\begin{aligned} & e^{\jmath\varpi_p \cos(\theta - \psi_{p,m})} + e^{\jmath\varpi_p \cos(\theta + \psi_{p,m})} \\ & \approx \sum_{n=0}^{N} J'_n(\varpi_p)\{\cos[n(\theta - \psi_{p,m})] + \cos[n(\theta + \psi_{p,m})]\} \\ & = \sum_{n=0}^{N} 2J'_n(\varpi_p)\cos(n\theta)\cos(n\psi_{p,m}). \end{aligned} \quad (31)$$

Substituting (31) into (26), we obtain an approximation of the beampattern:

$$\begin{aligned} & \mathcal{B}_N[\underline{\mathbf{h}}(\omega), \theta] \\ & = \sum_{p=1}^{P}\sum_{m=1}^{\mathcal{M}_p} H'^{*}_{p,m}(\omega) \sum_{n=0}^{N} 2J'_n(\varpi_p)\cos(n\theta)\cos(n\psi_{p,m}) \\ & = \sum_{p=1}^{P}\sum_{m=1}^{\mathcal{M}_p} H'_{p,m}(\omega) \sum_{n=0}^{N} 2J'^{*}_n(\varpi_p)\cos(n\theta)\cos(n\psi_{p,m}) \\ & = \sum_{n=0}^{N} \cos(n\theta)\left[2\sum_{p=1}^{P} J'^{*}_n(\varpi_p)\sum_{m=1}^{\mathcal{M}_p}\cos(n\psi_{p,m})H'_{p,m}(\omega)\right] \\ & = \sum_{n=0}^{N} b_{N,n}\cos(n\theta), \end{aligned} \quad (32)$$

where

$$b_{N,n} = 2\sum_{p=1}^{P} J'^{*}_n(\varpi_p)\sum_{m=1}^{\mathcal{M}_p}\cos(n\psi_{p,m})H'_{p,m}(\omega). \quad (33)$$

This clearly shows the desired relation.

We observe from (29) that as long as $e^{\jmath\varpi_p \cos(\theta \pm \psi_{p,m})}$ can be approximated by a Jacobi-Anger expansion of order N, we can build any Nth-order DMA with UCCAs. To better illustrate this, we give the truncation error of $e^{\jmath\varpi_p \cos(\theta \pm \psi_{p,m})}$ introduced by the Jacobi-Anger expansion. For simplicity, we consider $\psi_{p,m} = 0$ and define the truncation error as

$$\epsilon_N(\varpi_p) \triangleq \left| e^{\jmath\varpi_p \cos\theta} - \sum_{n=0}^{N} J'_n(\varpi_p)\cos(n\theta) \right|. \quad (34)$$

Figure 2 displays this error as a function of the order N, for different frequencies ($f = 500$ Hz and 1000 Hz), with $r = 2.6$ cm and $\theta = 0$. It is seen that for $N \geq 2$, the truncation error is below -50 dB.

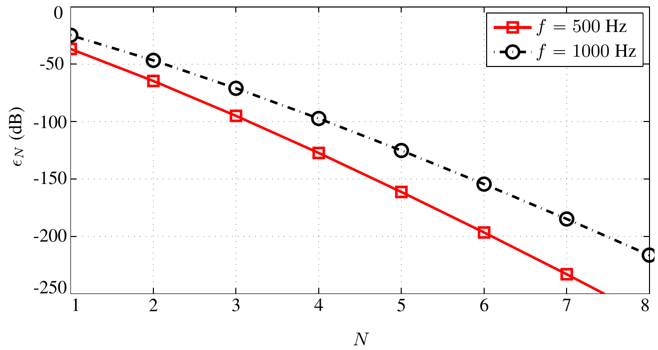

FIG. 2. (Color online) Illustration of the truncation error as a function of N, for different frequencies ($f = 500$ Hz and 1000 Hz), with $r = 2.6$ cm and $\theta = 0$.

V. DESIGN OF CDMA, ROBUST CDMA, AND ROBUST CCDMAS

We observe from (33) that the filter coefficients $H'_{p,m}(\omega)$, can be determined given the coefficients $b_{N,n}$. In this section, we show how to design robust CCDMAs based on this relationship. But before continuing on, we first briefly review the design of the conventional and robust CDMAs, which also serves as the motivation why CCDMAs are needed in practical applications.

A. Conventional CDMA

Conventional CDMAs are designed with a single ring, i.e., $P = 1$, then (33) becomes

$$b_{N,n} = 2J'^{*}_n(\varpi)\sum_{m=1}^{\mathcal{M}}\cos(n\psi_m)H'_m(\omega). \quad (35)$$

Note that the underline and subscripts are dropped from variables in this particular case as we only deal with one ring.

To design an Nth-order CDMA with the conventional approach, the number of microphones should satisfy $\mathcal{M} = N + 1$. From (35), we observe that the filter coefficients can be derived with the following equation (Benesty et al., 2014):

$$\Psi_{\mathcal{M}}(\omega)\mathbf{h}'(\omega) = \mathbf{b}_{N+1}, \quad (36)$$

where

$$\Psi_{\mathcal{M}}(\omega) \triangleq \begin{bmatrix} J'^{*}_0(\varpi) & J'^{*}_0(\varpi) & \cdots & J'^{*}_0(\varpi) \\ J'^{*}_1(\varpi) & J'^{*}_1(\varpi)\cos\psi_2 & \cdots & J'^{*}_1(\varpi)\cos\psi_{\mathcal{M}} \\ \vdots & \vdots & \cdots & \vdots \\ J'^{*}_N(\varpi) & J'^{*}_N(\varpi)\cos(N\psi_2) & \cdots & J'^{*}_N(\varpi)\cos(N\psi_{\mathcal{M}}) \end{bmatrix} \quad (37)$$

is a matrix of size $(N+1) \times \mathcal{M}$,

$$\mathbf{h}'(\omega) \triangleq \left[H'_1(\omega) \quad H'_2(\omega) \quad \cdots \quad H'_{\mathcal{M}}(\omega) \right]^T \tag{38}$$

is a vector of length $\mathcal{M}$, and

$$\mathbf{b}_{N+1} \triangleq \frac{1}{2} \left[b_{N,0} \quad b_{N,1} \quad \cdots \quad b_{N,N} \right]^T \tag{39}$$

is a vector of length $N+1$. It is easy to see $\boldsymbol{\Psi}_{\mathcal{M}}(\omega)$ is a full-rank square matrix and the solution to (36) is

$$\mathbf{h}'(\omega) = \boldsymbol{\Psi}_{\mathcal{M}}^{-1}(\omega)\mathbf{b}_{N+1}. \tag{40}$$

Given the filter $\mathbf{h}'(\omega)$, the global filter $\mathbf{h}(\omega)$ is easily constructed according to (27).

The conventional CDMA beamforming filter given by (40) suffers from two major problems, which prevent it from being used in practical systems: white noise amplification and significant SNR gain degradation at some frequencies. Some examples of these problems will be given in Sec. VI, e.g., Figs. 5 and 9 in Sec. VI. In Sec. V B and V C, we will discuss two approaches that can deal with these problems: one is to increase the number of microphone sensors in the design of an Nth-order CDMA, i.e., using more than $N+1$ sensors, and the other is to consider the use of a CCDMA.

B. Robust CDMA

It is well known that the conventional CDMA suffers from white noise amplification and the amount of white noise amplification is inversely proportional to the frequency. In other words, the white-noise-amplification problem becomes more serious at low frequencies (Benesty and Chen, 2012).

To improve the robustness of CDMA with respect to spatially white noise, a robust version of CDMA design approach is developed, which improves the robustness by increasing the number of microphones, i.e., $\mathcal{M} > N+1$, in which the beamformer is derived by maximizing the WNG (Benesty *et al.*, 2014). This is equivalent to minimizing $\mathbf{h}'^H(\omega)\mathbf{h}'(\omega)$ subject to the constraint in (36), i.e.,

$$\min_{\mathbf{h}'(\omega)} \mathbf{h}'^H(\omega)\mathbf{h}'(\omega) \ \text{ s.t. } \ \Psi(\omega)\mathbf{h}'(\omega) = \mathbf{b}_{N+1}. \tag{41}$$

Solving the above optimization problem (Benesty and Chen, 2012), we obtain the minimum-norm CDMA beamforming filter:

$$\mathbf{h}'(\omega) = \Psi_{\mathcal{M}}^H(\omega)\left[\Psi_{\mathcal{M}}(\omega)\Psi_{\mathcal{M}}^H(\omega)\right]^{-1}\mathbf{b}_{N+1}. \tag{42}$$

Again, with the filter $\mathbf{h}'(\omega)$, the global filter $\mathbf{h}(\omega)$ is constructed according to (27).

As shown ın Benesty *et al.* (2014) as well as in this minimum-norm filter is able to increase the WNG. For a specified order of CDMA, the more the microphones are used, the higher is the WNG.

C. Robust CCDMA

Besides the white-noise-amplification problem, the conventional CDMA may also suffer from significant degradation in SNR gains at some frequencies, i.e., deep nulls in the SNR gains at some frequencies as shown in Sec. VI. This is due to spatial aliasing and those nulls are introduced by the zeros in the denominators of the filter coefficients, i.e., the zeros of the Bessel function, $J_n(\varpi)$. In the design of an Nth-order CDMA, a zero of any order Bessel function causes a null and make the CDMA suffer from serious performance degradation. The minimum-norm filter improves the WNG by fully exploiting the fact that we have more microphones than required for a given CDMA order. However, more microphones often means a larger array aperture (radius), which introduces more nulls and make the nulls move toward lower frequencies.

To solve the nulls problem, we propose a robust approach with CCDMA. Considering a UCCA with P rings, we get the following equation:

$$\underline{\Psi}(\omega)\underline{\mathbf{h}}'(\omega) = \mathbf{b}_{N+1}, \tag{43}$$

where

$$\underline{\Psi}(\omega) \triangleq \left[\Psi_1(\omega) \quad \Psi_2(\omega) \quad \cdots \quad \Psi_P(\omega) \right] \tag{44}$$

is a matrix of size $(N+1) \times \underline{\mathcal{M}}$ (where $\underline{\mathcal{M}} = \sum_{p=1}^{P} \mathcal{M}_p$),

$$\Psi_p \triangleq \begin{bmatrix} J'^*_0(\varpi_p)\gamma_{p,0}^T \\ J'^*_1(\varpi_p)\gamma_{p,1}^T \\ \vdots \\ J'^*_N(\varpi_p)\gamma_{p,N}^T \end{bmatrix} \tag{45}$$

is a matrix of size $(N+1) \times \mathcal{M}_p$, with

$$\gamma_{p,n} \triangleq \left[1 \quad \cos(n\psi_{p,2}) \quad \cdots \quad \cos(n\psi_{p,\mathcal{M}_p}) \right]^T, \quad n = 0,1,2,\ldots,N, \ p = 1,2,\ldots,P \tag{46}$$

and

$$\underline{\mathbf{h}}'(\omega) \triangleq \left[\mathbf{h}'^T_1(\omega) \quad \mathbf{h}'^T_2(\omega) \quad \cdots \quad \mathbf{h}'^T_P(\omega) \right]^T \tag{47}$$

is a vector of length $\underline{\mathcal{M}}$, with

$$\mathbf{h}'_p(\omega) \triangleq \left[H'_{p,1}(\omega) \quad H'_{p,2}(\omega) \quad \cdots \quad H'_{p,\mathcal{M}_p}(\omega) \right]^T \tag{48}$$

being a vector of length $\mathcal{M}_p$.

In a similar way, we obtain the minimum-norm filter:

$$\underline{\mathbf{h}}'(\omega) = \underline{\Psi}^H(\omega)\left[\underline{\Psi}(\omega)\underline{\Psi}^H(\omega)\right]^{-1}\mathbf{b}_{N+1}. \tag{49}$$

After $\underline{\mathbf{h}}'(\omega)$, $\mathbf{h}_p(\omega)$, $p = 1,2,\ldots,P$ are computed according to (27), The global filter $\underline{\mathbf{h}}(\omega)$ is then formed according to (10). We call this beamformer the robust CCDMA. It can be checked that this filter degenerates to the conventional CDMA in (40) if $P=1$ and $\mathcal{M}_1 = N+1$. For $P=1$ and $\mathcal{M}_1 > N+1$, it degenerates to the robust CDMA given in (42).

D. Design example

To better illustrate the performance improvement with the robust CCDMA, we give an example of the design of the first-order CCDMA, i.e., $N=1$.

From (44)–(46), it is not difficult to verify that

$$\underline{\Psi}(\omega)\underline{\Psi}^H(\omega) = \begin{bmatrix} \chi_{11}(\omega) & \chi_{12}(\omega) \\ \chi_{12}^*(\omega) & \chi_{22}(\omega) \end{bmatrix}, \tag{50}$$

where

$$\begin{aligned} \chi_{11}(\omega) &\triangleq \sum_{p=1}^{P} \mathcal{M}_p |J'_0(\varpi_p)|^2, \\ \chi_{12}(\omega) &\triangleq \sum_{p=1}^{P} J'_0(\varpi_p) J'^*_1(\varpi_p) \sum_{m=1}^{\mathcal{M}_p} \cos\psi_{p,m}, \\ \chi_{22}(\omega) &\triangleq \sum_{p=1}^{P} |J'_1(\varpi_p)|^2 \sum_{m=1}^{\mathcal{M}_p} \cos^2\psi_{p,m}. \end{aligned} \tag{51}$$

In this example, we assume that M_p is an even number, then $\mathcal{M}_p = \lfloor M_p/2 \rfloor + 1 = M_p/2 + 1$, so $M_p = 2(\mathcal{M}_p - 1)$, and

$$\psi_{p,m} = \frac{2\pi(m-1)}{M_p} = \frac{\pi(m-1)}{\mathcal{M}_p - 1}. \tag{52}$$

It follows then that

$$\begin{aligned} &\sum_{m=1}^{\mathcal{M}_p} \cos\psi_{p,m} = 0, \\ &\sum_{m=1}^{\mathcal{M}_p} \cos^2\psi_{p,m} = \frac{(\mathcal{M}_p + 1)}{2}. \end{aligned} \tag{53}$$

Substituting (53) into (51), we get

$$\begin{aligned} &\chi_{12}(\omega) = 0, \\ &\chi_{22}(\omega) = \frac{1}{2}\sum_{p=1}^{P} (\mathcal{M}_p + 1)|J'_1(\varpi_p)|^2. \end{aligned} \tag{54}$$

Consequently, we have

$$\left[\underline{\Psi}(\omega)\underline{\Psi}^H(\omega)\right]^{-1} = \begin{bmatrix} \dfrac{1}{\sum_{p=1}^{P} \mathcal{M}_p |J'_0(\varpi_p)|^2} & 0 \\ 0 & \dfrac{2}{\sum_{p=1}^{P} (\mathcal{M}_p + 1)|J'_1(\varpi_p)|^2} \end{bmatrix}. \tag{55}$$

Substituting (55) and (30) into (49), we obtain

$$\begin{aligned} H'_{p,m}(\omega) = {} & \frac{b_{1,0} J_0(\varpi_p)}{2\sum_{p=1}^{P} \mathcal{M}_p J_0^2(\varpi_p)} \\ & + \jmath \frac{b_{1,1} J_1(\varpi_p) \cos\psi_{p,m}}{\sum_{p=1}^{P} (\mathcal{M}_p + 1) J_1^2(\varpi_p)}, \\ & m = 1, 2, \ldots, \mathcal{M}_p, \quad p = 1, 2, \ldots, P. \end{aligned} \tag{56}$$

We see that the denominators of the filter coefficients in (56) are a function of combined squared Bessel functions, i.e., $\sum_p \mathcal{M}_p J_0^2(\varpi_p)$ and $\sum_p (\mathcal{M}_p + 1) J_1^2(\varpi_p)$. For $P = 1$, it is clearly seen that the zeros of the Bessel function in the denominator of the filter coefficients leads to nulls. In fact, it is easy to see that the zeros' positions in $J_n(\varpi_p)$ are determined by $\varpi_p = \omega r_p / c$, which is a function of ω and the radius r_p. For a specified frequency ω, the larger the array aperture (radius), the more serious is the nulls problem.

From the above analysis, one can conclude that increasing the number of microphones may worsen the nulls problem since more microphones often means a larger array aperture (radius). Clearly, one way to avoid the nulls problem is by decreasing the value of the radius. However, in practice, the smallest value of radius depends on the total number of sensors and the physical size of microphone sensors and it cannot be too small. Moreover, decreasing the radius means a smaller interelement spacing, which leads to more severe white noise amplification.

The robust CCDMA can improve the performance. The fundamental reason is that a UCCA combines different rings together with appropriate radii and the denominators in the filter coefficients are also a combination of different Bessel functions. Since the zeros of the Bessel functions (with different radii) are occurring at different positions (frequencies), the combined function generally does not have zeros. Consequently, the performance degradation caused by the nulls can be improved significantly.

Figure 3 shows the normalized value (with respect to the maximum value) of the combined squared zero- and first-order Bessel functions with a UCCA. As one can see, when only one ring is used ($P = 1$, $M = 8$, $r = 3.7$ cm), there are three zeros in the frequency range from 0 Hz to 8 kHz. When two ($P = 2$, $M_1 = 6$, $r_1 = 2.0$ cm, $M_2 = 8$, $r_2 = 3.7$ cm) or three ($P = 3$, $M_1 = 4$, $r_1 = 1.5$ cm, $M_2 = 6$, $r_2 = 2.0$ cm, $M_3 = 8$, $r_3 = 3.7$ cm) rings are used, the zeros vanish. A more detailed study on this will be shown with a set of simulations in Sec. V E.

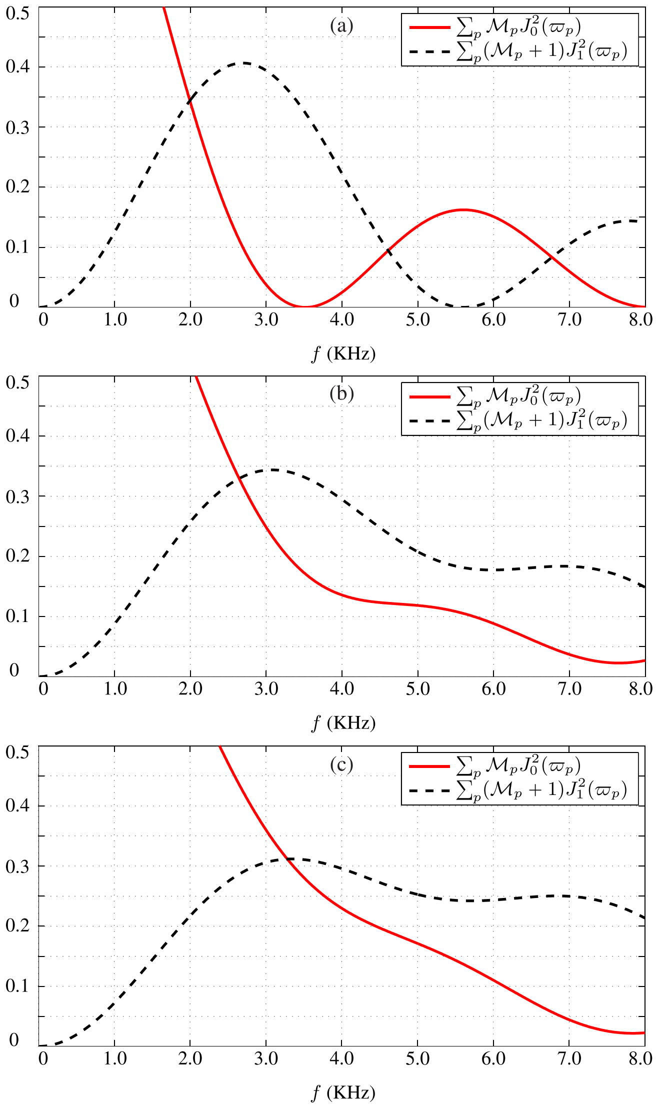

FIG. 3. (Color online) Normalized value of the combined squared zero- and first-order Bessel functions with a UCCA: (a) $P=1$, (b) $P=2$, and (c) $P=3$.

E. Criterion to determine the radii of different rings

Besides beamforming, another important problem in designing a CCDMA is to determine the values of the radii of the different rings so that the nulls in the DF or WNG would not happen. Let us consider a first-order CCDMA with two rings and the radii of the first and second rings are denoted as r_1 and r_2, respectively. For the first ring, let us assume that the first three zeros (the other zeros occur at higher frequencies, which are out of the frequency band of interest) of $J_0(\varpi)$ are, respectively,

$$\varpi_{1,0,1}=\omega_{0,1}r_1/c,\quad \varpi_{1,0,2}=\omega_{0,2}r_1/c,\quad \varpi_{1,0,3}=\omega_{0,3}r_1/c, \tag{57}$$

where the three digits in the subscript denotes, respectively, the ring number, the Bessel function order, and the zero number, respectively.

Similarly, we assume that the first three zeros of the $J_0(\varpi)$ for the second ring are

$$\varpi_{2,0,1}=\omega_{0,1}r_2/c,\quad \varpi_{2,0,2}=\omega_{0,2}r_2/c,\quad \varpi_{2,0,3}=\omega_{0,3}r_2/c. \tag{58}$$

As discussed in Sec. V D, the denominators in the CCDMA filter coefficients are a combination of different Bessel functions. To ensure that the sum of the Bessel functions does not have zeros, the zeros of the Bessel functions with different radii must occur at different positions (frequencies). Therefore, we should have

$$\varpi_{2,0,1}\neq\varpi_{1,0,2},\quad \varpi_{2,0,1}\neq\varpi_{1,0,3},\quad \varpi_{2,0,2}\neq\varpi_{1,0,3}, \tag{59}$$

which means that

$$r_2\neq\frac{\omega_{0,2}}{\omega_{0,1}}r_1,\quad r_2\neq\frac{\omega_{0,3}}{\omega_{0,1}}r_1,\quad r_2\neq\frac{\omega_{0,3}}{\omega_{0,2}}r_1. \tag{60}$$

In a similar manner and with $J_1(\varpi)$, one can find that

$$r_2\neq\frac{\omega_{1,2}}{\omega_{1,1}}r_1,\quad r_2\neq\frac{\omega_{1,3}}{\omega_{1,1}}r_1,\quad r_2\neq\frac{\omega_{1,3}}{\omega_{1,2}}r_1. \tag{61}$$

Putting (59) and (60), we find the condition for the first-order CCDMA not having any zero in DF or WNG:

$$\frac{r_2}{r_1}\notin\left[\frac{\omega_{0,2}}{\omega_{0,1}},\ \frac{\omega_{0,3}}{\omega_{0,1}},\ \frac{\omega_{0,3}}{\omega_{0,2}},\ \frac{\omega_{1,2}}{\omega_{1,1}},\ \frac{\omega_{1,3}}{\omega_{1,1}},\ \frac{\omega_{1,3}}{\omega_{1,2}}\right]. \tag{62}$$

The above analysis can be easily generalized to a first-order CCDMA with any number of rings. Theoretically, at least two rings are needed in order to avoid nulls in the DF. The above criteria can also be generalized to analyze higher order CCDMAs ($N\geq 2$), which is more complicated and will not be presented here.

VI. PERFORMANCE EVALUATION

In this section, we briefly study through simulations the performance of the conventional, robust CDMA, and robust CCDMA. To make the paper concise, we only focus on the design of the supercardioid.

A. Performance study

We first study the performance of the conventional and robust CDMAs, and the robust CCDMA to design the second-order supercardioid. The parameters of the

TABLE I. Parameters of the second-order supercardioid and design parameters.

Second-Order Supercardioid	
Directivity Pattern: $\mathcal{B}_2(\theta)=0.309+0.484\cos\theta+0.207\cos(2\theta)$	
Conventional CDMA	$M=4$, $r=2$ cm
Robust CDMA	$M=8$, $r=3.7$ cm
Robust CCDMA	M_1=4, r_1=2 cm M_2=8, r_2=3.7 cm

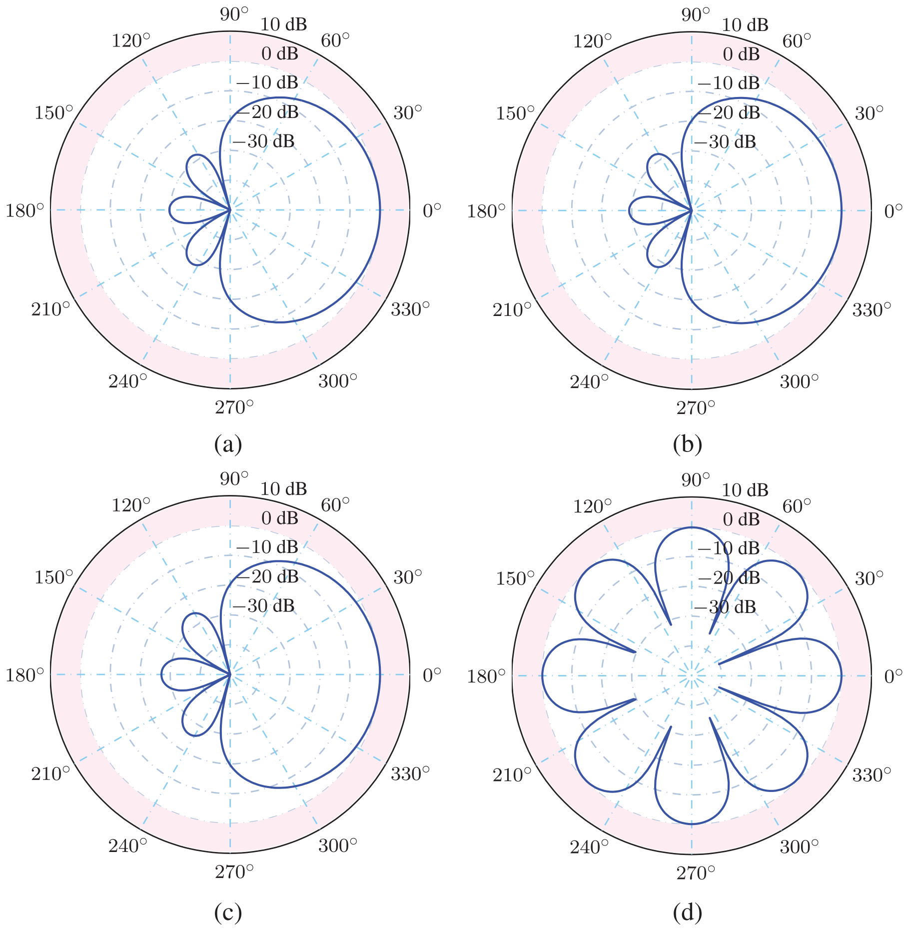

FIG. 4. Beampatterns of the conventional CDMA: (a) $f = 500\,\text{Hz}$, (b) $f = 1000\,\text{Hz}$, (c) $f = 2000\,\text{Hz}$, and (d) $f = 6500\,\text{Hz}$. Conditions of simulation: $M = 4$, $r = 2.0\,\text{cm}$, and the desired beampattern is the second-order supercardioid.

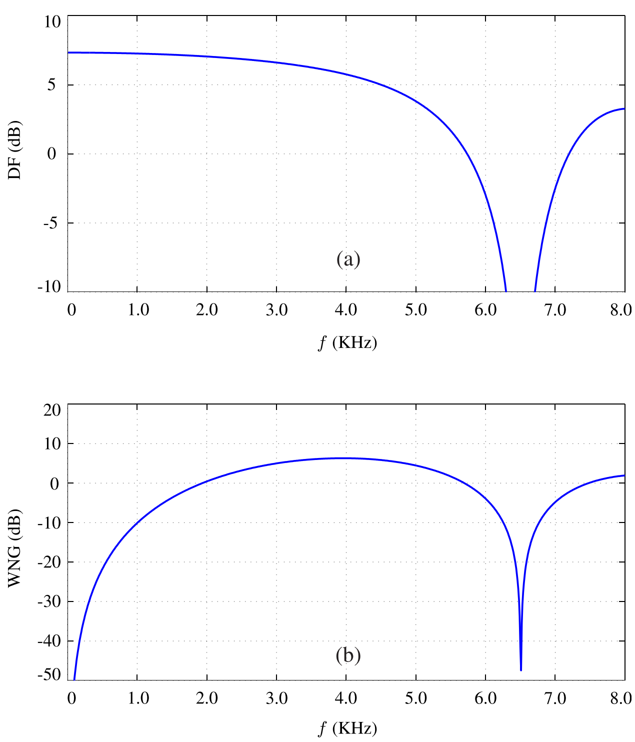

FIG. 5. (Color online) SNR gains of the conventional CDMA: (a) DF and (b) WNG. Conditions of simulation: $M = 4$, $r = 2.0\,\text{cm}$, and the desired beampattern is the second-order supercardioid.

second-order supercardioid as well as of those for the design of the CDMA and the CCDMA are listed in Table I. Performance is evaluated with respect to beampattern, DF, and WNG.

Figures 4 and 5 show the beampattern, DF, and WNG of the conventional CDMA with four microphones. As we can see, the conventional CDMA has almost frequency-invariant beampatterns at low but not at high frequencies. When $f = 6500\,\text{Hz}$, the beampattern is considerably changed, because of spatial aliasing. Figure 5 shows that the beamformer has a very low WNG at low frequencies, indicating that this beamformer significantly amplifies white noise at low frequencies. As the frequency increases, the WNG improves; however, both the DF and WNG suffer from significant performance degradation near the null's position, i.e., at $f = 6500\,\text{Hz}$. In other words, the conventional CDMA suffers from both white noise amplification and spatial aliasing even with a small array radius, which limit the potential of this beamformer in practice.

We then study the performance of the robust CDMA with eight microphones. The corresponding beampattern, DF, and WNG are plotted in Figs. 6 and 7. As can be seen, the robust CDMA greatly improves the WNG, especially at low frequencies, as compared to the conventional CDMA. However, this beamformer uses more microphones; as a result, the increase of the radius leads to more nulls in the frequency band of interest and makes the nulls' positions

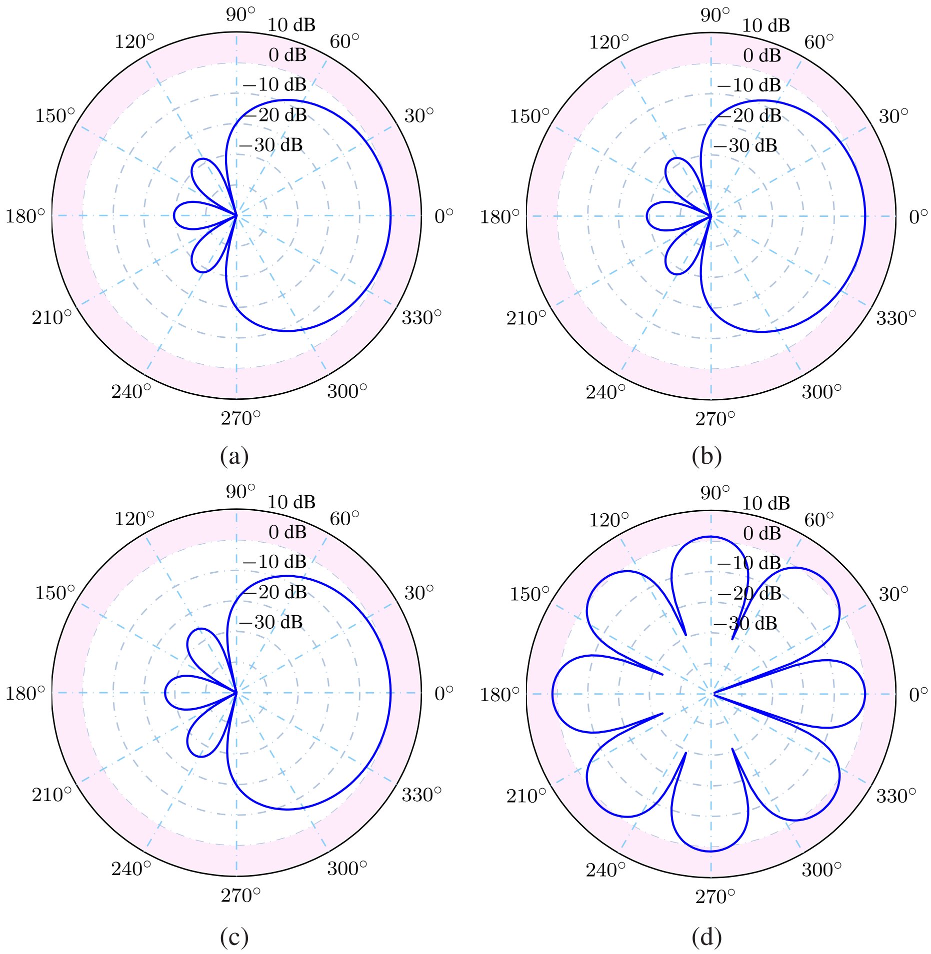

FIG. 6. (Color online) Beampatterns of the robust CDMA: (a) $f = 500$ Hz, (b) $f = 1000$ Hz, (c) $f = 2000$ Hz, and (d) $f = 3520$ Hz. Conditions of simulation: $M = 8$, $r = 3.7$ cm, and the desired beampattern is the second-order supercardioid.

move to lower frequencies. Indeed, Fig. 6 shows that the beampattern has already suffered tremendous change at $f = 3520$ Hz and Fig. 7 shows that there are three nulls in the frequency band of interest.

Figures 8 and 9 shows the performance of the robust CCDMA with two rings. Figure 8 shows that the robust CCDMA has almost frequency-invariant beampatterns at all frequencies. Figure 9 shows that both the DF and the WNG have reasonable performance in the frequency band of interest. This illustrates that the robust CCDMA not only greatly improves the WNG but also mitigates the nulls problem.

As shown by Benesty *et al.* (2014), CDMAs can perfectly steer at least in M different directions (i.e., at the positions of the microphones) due to the symmetrical property of the geometry, and the filters corresponding to those directions are easily obtained by simply permuting the coefficients of the filter designed for $\theta_s = 0$. Similarly, to ensure that the robust CCDMA can perfectly steer to these directions, the symmetry property in those directions is needed. So, it is better to make the geometry of the UCCA satisfy $M_2 = kM_1$, where $k = 1, 2, 3, \ldots$. In this way, the robust CCDMA can perfectly steer in M_1 different directions (where microphones in the two rings are aligned), i.e., $2\pi(m-1)/M_1$. Figure 10 plots the beampatterns of the robust CCDMA with $\theta_s \in \{0°, 90°, 180°, 270°\}$. As can be seen, the robust CCDMA has the same beampattern in the aforementioned directions.

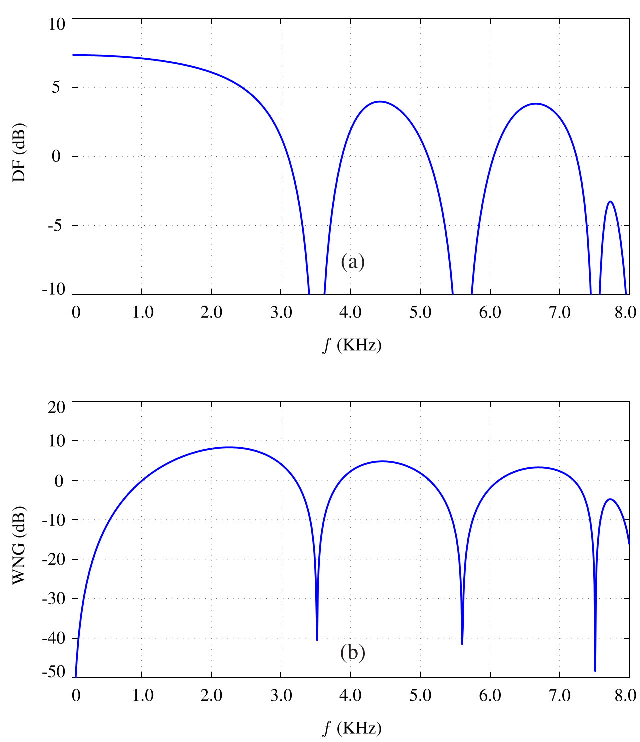

FIG. 7. (Color online) SNR gains of the robust CDMA: (a) DF and (b) WNG. Conditions of simulation: $M = 8$, $r = 3.7$ cm, and the desired beampattern is the second-order supercardioid.

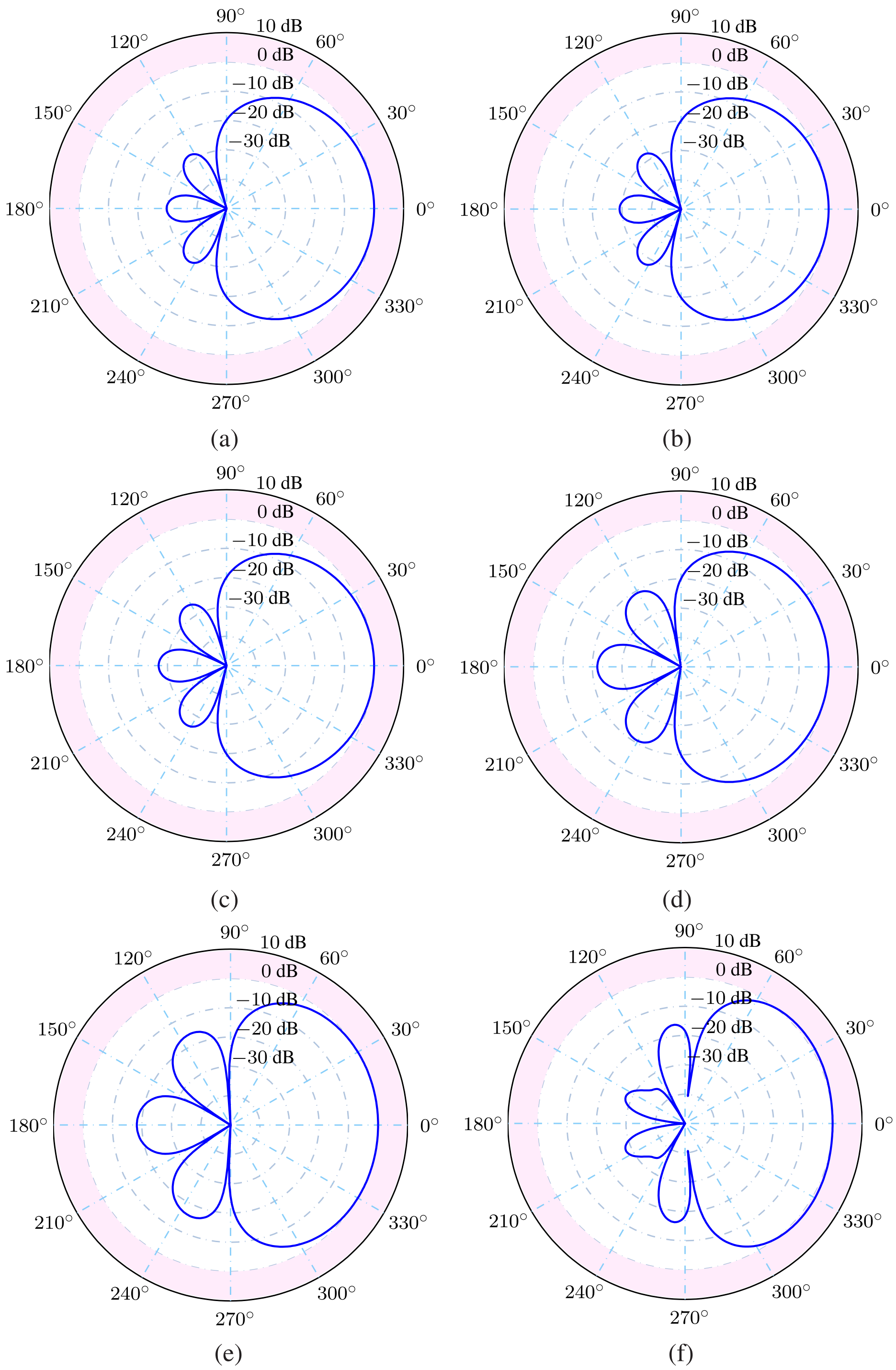

FIG. 8. (Color online) Beampatterns of the robust CCDMA: (a) $f = 500$ Hz, (b) $f = 1000$ Hz, (c) $f = 2000$ Hz, (d) $f = 3520$ Hz, (e) $f = 5000$ Hz, and (f) $f = 6500$ Hz. Conditions of simulation: $M_1 = 4$, $M_2 = 8$, $r_1 = 2$ cm, $r_2 = 3.7$ cm, and the desired beampattern is the second-order supercardioid.

B. Performance comparison

To better demonstrate the performance improvement with the robust CCDMA, we compare the following:

(1) The conventional CDMA;
(2) The robust CDMA which has the same interelement spacing as the conventional CDMA (we call it the robust CDMA-I);
(3) The robust CCDMA (with two rings), in which the first ring has the same geometry as the conventional CDMA while the second one has the same geometry as the robust CDMA-I; and
(4) The robust CDMA which has the same number of microphones as the robust CCDMA while the radius remains the same as the robust CDMA-I (we call it the robust CDMA-II), to design the second-order supercardioid. The parameters for the design of the conventional CDMA, robust CDMA-I, and robust CCDMA are listed in Table I. The robust CDMA-II is designed with $M = 12$ and $r = 3.7$ cm.

The results (DF, WNG, and zoomed plot of the WNG at low frequencies) are plotted in Fig. 11. It is clearly seen, besides the white-noise-amplification problem, the conventional CDMA

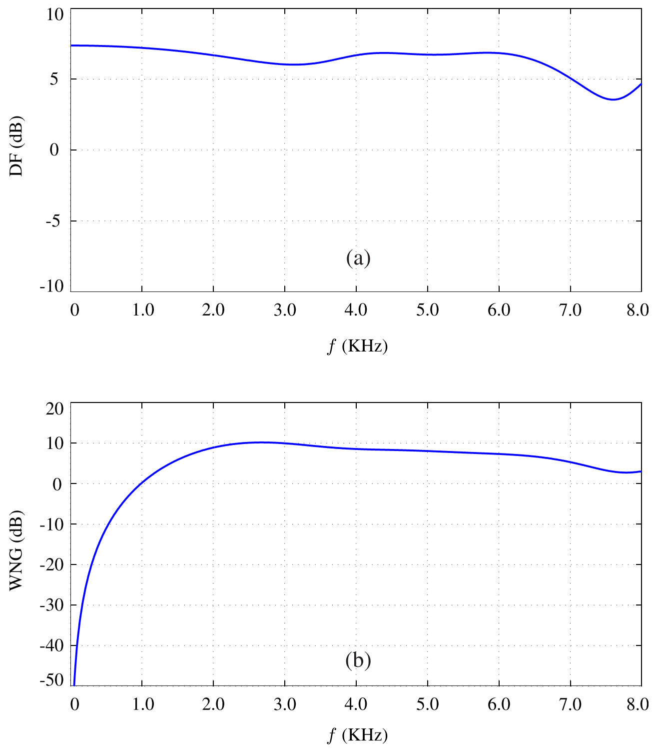

FIG. 9. (Color online) SNR gains of the robust CCDMA: (a) DF and (b) WNG. Conditions of simulation: $M_1 = 4$, $M_2 = 8$, $r_1 = 2$ cm, $r_2 = 3.7$ cm, and the desired beampattern is the second-order supercardioid.

also suffers from serious degradation in SNR gain due to the nulls problem as discussed in Sec. V. While the robust CDMA approach can improve the WNG, the increase of the array aperture (radius) leads to more nulls in the frequency range of interest. Moreover, it is seen that both the robust CDMA-I and CDMA-II have almost the same performance in SNR gain, which means that increasing the number of microphones and keeping the same value of the radius may not improve the WNG. In comparison, the robust CCDMA achieves a significant better performance. It improves the WNG and does not have any null, where the DF and the WNG remain approximately constant in the frequency band of interest. This demonstrates the advantages of the robust CCDMA.

VII. CONCLUSIONS

This paper studied the design of CDMAs and CCDMAs and the associated beamforming problem. While they have the potential to form frequency-invariant directivity patterns and have good steering flexibility, the traditional CDMAs suffer from both white noise amplification and serious nulls problem in SNR gain due to spatial aliasing. The so-called robust CDMAs can help improve WNG by using more sensors than required for the order of the differential array; however, this robust method does not improve and may even worsen the SNR gain nulls problem. In this paper, we

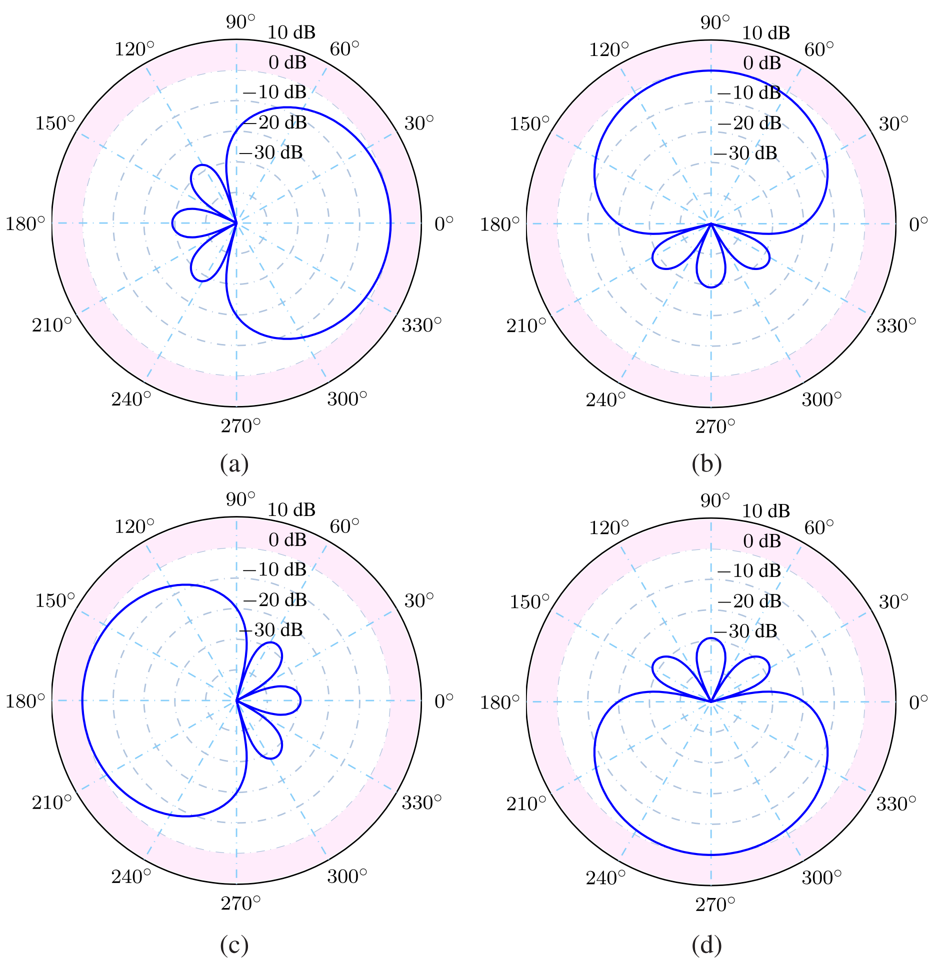

FIG. 10. (Color online) Beampatterns of the robust CCDMA: (a) $\theta_s = 0°$, (b) $\theta_s = 90°$, (c) $\theta_s = 180°$, and (d) $\theta_s = 270°$. Conditions of simulation: $M_1 = 4$, $M_2 = 8$, $r_1 = 2$ cm, $r_2 = 3.7$ cm, $f = 1000$ Hz, and the desired beampattern is the second-order supercardioid.

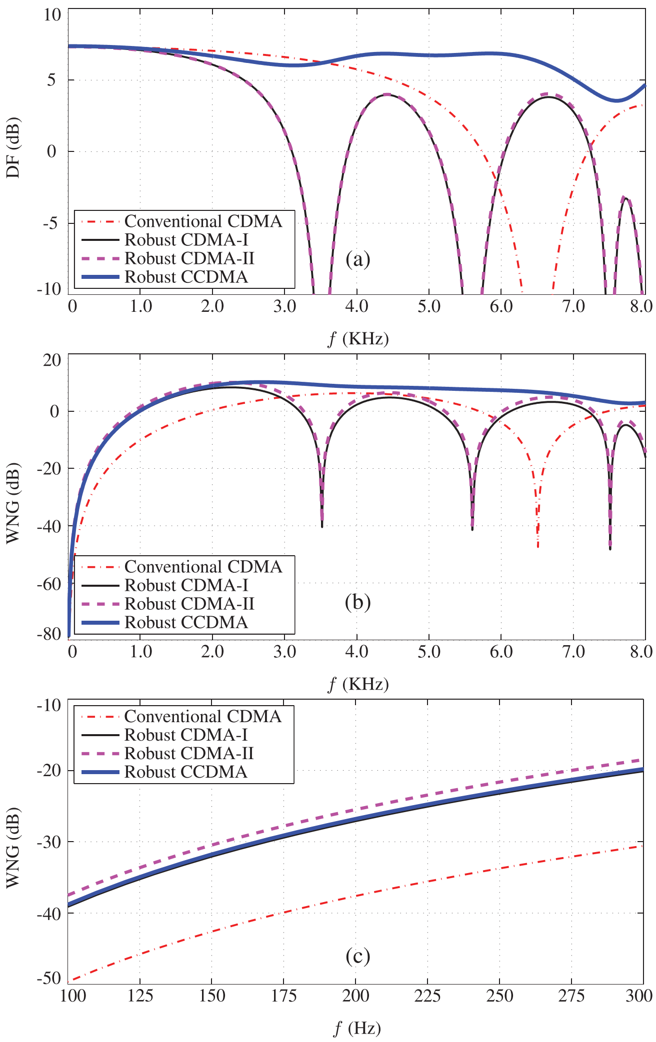

FIG. 11. SNR gains of the conventional, robust CDMA, and robust CCDMA for the design of the second-order supercardioid: (a) DF, (b) WNG, and (c) zoomed plot of the WNG at low frequencies.

performed some theoretical analysis of the nulls problem and found that the nulls of the CDMAs are caused by the zeros of the Bessel function in the denominators of the filters' coefficients. We then developed a robust CCDMA approach, which combines different rings of microphones together with appropriate radii. Simulation results demonstrated the superiority of the robust CCDMA approach over the traditional and robust CDMAs: it can mitigate both the problem of white noise amplification and the nulls problem with CDMAs.

ACKNOWLEDGMENT

This work was supported in part by the NSFC "Distinguished Young Scientists Fund" under Grant No. 61425005.

[1]This noise models the sensors' self noise.

Abhayapala, T. D., and Gupta, A. (**2010**). "Higher order differential-integral microphone arrays," J. Acoust. Soc. Am. **136**, 227–233.
Abramowitz, M., and Stegun, I. A. (**1972**). *Handbook of Mathematical Functions with Formulas, Graphs, and Mathematical Tables* (Dover Publications, Mineola, New York), 1046 pp.
Balmages, I., and Rafaely, B. (**2007**). "Open-sphere designs for spherical microphone arrays," IEEE Trans. Audio Speech Lang. Process. **15**, 727–732.
Benesty, J., and Chen, J. (**2012**). *Study and Design of Differential Microphone Arrays* (Springer-Verlag, Berlin, Germany), 182 pp.
Benesty, J., Chen, J., and Cohen, I. (**2014**). *Design of Circular Differential Microphone Arrays* (Springer-Verlag, Berlin, Germany), 166 pp.
Benesty, J., Chen, J., and Huang, Y. (**2008**). *Microphone Array Signal Processing* (Springer-Verlag, Berlin, Germany), 232 pp.
Benesty, J., and Gänsler, T. (**2002**). "A multichannel acoustic echo canceler double-talk detector based on a normalized cross-correlation matrix," Eur. Trans. Telecomm. **13**, 95–101.
Benesty, J., Souden, M., and Huang, Y. (**2012**). "A perspective on differential microphone arrays in the context of noise reduction," IEEE Trans. Audio Speech Lang. Process. **20**, 699–704.
Berkun, R., Cohen, I., and Benesty, J. (**2015**). "Combined beamformers for robust broadband regularized superdirective beamforming," IEEE/ACM Trans. Audio Speech Lang. Process. **23**, 877–886.
Brandstein, M., and Ward, D. (**2001**). *Microphone Arrays: Signal Processing Techniques and Applications* (Springer-Verlag, Berlin, Germany), 398 pp.
Capon, J. (**1969**). "High-resolution frequency-wavenumber spectrum analysis," Proc. IEEE **57**, 1408–1418.
Chan, S., and Chen, H. (**2007**). "Uniform concentric circular arrays with frequency-invariant characteristics: Theory, design, adaptive beamforming and DOA estimation," IEEE Trans. Signal Process. **55**, 165–177.
Cox, H., Zeskind, R., and Owen, M. (**1987**). "Robust adaptive beamforming," IEEE Trans. Acoust. Speech Signal Process. **35**, 1365–1376.
Crocco, M., and Trucco, A. (**2011**). "Design of robust superdirective arrays with a tunable tradeoff between directivity and frequency-invariance," IEEE Trans. Signal Process. **59**, 2169–2181.
Doclo, S., and Moonen, M. (**2007**). "Superdirective beamforming robust against microphone mismatch," IEEE Trans. Audio Speech Lang. Process. **15**, 617–631.
Elko, G. W. (**1996**). "Microphone array systems for hands-free telecommunication," Speech Commun. **20**, 229–240.
Elko, G. W. (**2004**). "Differential microphone arrays," in *Audio Signal Processing for Next-Generation Multimedia Communication Systems*, edited by Y. Huang and J. Benesty (Kluwer Academic Publishers, Norwell, MA), Chap. 2, pp. 11–66.
Elko, G. W., and Meyer, J. (**2008**). "Microphone arrays," in *Springer Handbook of Speech Processing*, edited by J. Benesty, M. M. Sondhi, and Y. Huang (Springer-Verlag, Berlin, Germany), Chap. 48, pp. 1021–1041.
Frost, O. L., III (**1972**). "An algorithm for linearly constrained adaptive array processing," Proc. IEEE **60**, 926–935.
Gannot, S., Burshtein, D., and Weinstein, E. (**1999**). "Beamforming methods for multi-channel speech enhancement," in *Proc. IEEE IWAENC*, pp. 96–99.
Huang, G., Benesty, J., and Chen, J. (**2016**). "Subspace superdirective beamforming with uniform circular microphone arrays," in *Proc. IEEE IWAENC*, pp. 1–5.
Ihle, M. (**2003**). "Differential microphone arrays for spectral subtraction," in *Proc. IEEE IWAENC*, pp. 259–262.
Koyama, S., Furuya, K., Wakayama, K., Shimauchi, S., and Saruwatari, H. (**2016**). "Analytical approach to transforming filter design for sound field recording and reproduction using circular arrays with a spherical baffle," J. Acoust. Soc. Am. **139**, 1024–1036.
Li, C., Benesty, J., Huang, G., and Chen, J. (**2016**). "Subspace superdirective beamformers based on joint diagonalization," in *Proc. IEEE ICASSP*, Shanghai, China (March 20–25, 2016).
Markovich, S., Gannot, S., and Cohen, I. (**2009**). "Multichannel eigenspace beamforming in a reverberant noisy environment with multiple interfering speech signals," IEEE Trans. Audio Speech Lang. Process. **17**, 1071–1086.
Monzingo, R. A., and Miller, T. W. (**1980**). *Introduction to Adaptive Arrays* (SciTech Publishing, Raleigh, NC), 541 pp.
Olson, H. F. (**1946**). "Gradient microphones," J. Acoust. Soc. Am. **17**, 192–198.
Park, M., and Rafaely, B. (**2005**). "Sound-field analysis by plane-wave decomposition using spherical microphone array," J. Acoust. Soc. Am. **118**, 3094–3103.
Poletti, M. A. (**2000**). "A unified theory of horizontal holographic sound systems," J. Audio Eng. Soc. **48**, 1155–1182.

Quijano, J. E., and Zurk, L. M. (**2015**). "Eigenvector pruning method for high resolution beamforming," J. Acoust. Soc. Am. **138**, 2152–2160.

Rafaely, B. (**2005**). "Analysis and design of spherical microphone arrays," IEEE Trans. Speech Audio Process. **13**, 135–143.

Rafaely, B., Balmages, I., and Eger, L. (**2007**). "High-resolution plane-wave decomposition in an auditorium using a dual-radius scanning spherical microphone array," J. Acoust. Soc. Am. **122**, 2661–2668.

Sena, E. D., Hacihabiboglu, H., and Cvetkovic, Z. (**2012**). "On the design and implementation of higher-order differential microphones," IEEE Trans. Audio Speech Lang. Process. **20**, 162C174.

Shahbazpanahi, S., Gershman, A. B., Luo, Z.-Q., and Wong, K. M. (**2003**). "Robust adaptive beamforming for general-rank signal models," IEEE Trans. Signal Process. **51**, 2257–2269.

Sun, H., Kellermann, W., Mabande, E., and Kowalczyk, K. (**2012**). "Localization of distinct reflections in rooms using spherical microphone array eigenbeam processing," J. Acoust. Soc. Am. **131**, 2828–2840.

Teutsch, H. (**2007**). *Modal Array Signal Processing: Principles and Applications of Acoustic Wavefield Decomposition* (Springer-Verlag, Berlin, Germany), 253 pp.

Teutsch, H., and Elko, G. W. (**2001**). "First-and second-order adaptive differential microphone arrays," in *Proc. IEEE IWAENC*, pp. 35–38.

Teutsch, H., and Kellermann, W. (**2006**). "Acoustic source detection and localization based on wavefield decomposition using circular microphone arrays," J. Acoust. Soc. Am. **120**, 2724–2736.

Tiana-Roig, E., Jacobsen, F., and Fernandez-Grande, E. (**2011**). "Beamforming with a circular array of microphones mounted on a rigid sphere (L)," J. Acoust. Soc. Am. **130**, 1095–1098.

Tiana-Roig, E., Jacobsen, F., and Grande, E. F. (**2010**). "Beamforming with a circular microphone array for localization of environmental noise sources," J. Acoust. Soc. Am. **128**, 3535–3542.

Van Veen, B. D., and Buckley, K. M. (**1988**). "Beamforming: A versatile approach to spatial filtering," IEEE ASSP Mag. **5**, 4–24.

Wang, Y., Yang, Y., Ma, Y., and He, Z. (**2014**). "Robust high-order superdirectivity of circular sensor arrays," J. Acoust. Soc. Am. **136**, 1712–1724.

Yan, S. (**2015**). "Optimal design of modal beamformers for circular arrays," J. Acoust. Soc. Am. **138**, 2140–2151.

Zhao, L., Benesty, J., and Chen, J. (**2014**). "Design of robust differential microphone arrays," IEEE/ACM Trans. Audio Speech Lang. Process. **22**, 1455–1466.

Zhao, L., Benesty, J., and Chen, J. (**2016**). "Design of robust differential microphone arrays with the Jacobi–Anger expansion," Appl. Acoust. **110**, 194–206.